FTIR Spectra Analysis of Zinc Substituted Barium Nickel Ferrite

Sadiq. H. Khoreem, A. H. AL-Hammadi & W. F.Al-Eryani

Sana'a University

ABSTRACT

Nano - crystalline BaNix-2ZnxFe16O27 (where x = 0.0, 0.4, 0.8, 1.2, 1.6, and 2.0) w-type hexa-ferrite samples were generated using the typical standard ceramic methodology. Fourier transform infrared spectroscopy (FTIR) is a method which is used to identify the characteristic functional groups from the spectral bands that allow us to know the conjugation between the nanoparticles and the adsorbed biomolecules. It is used to detect different functional groups in Barium ferrites. The FTIR spectrum is recorded between 400 and 4000 cm−1. The result shows the two main bands of absorption. The high-frequency band in the range 550-600 cm- 1 and a low-frequency band at around 400 cm-1 were assigned to tetrahedral v1 and octahedral v2 sites, respectively, which illustrated the formation of the ferrite phase.

Keywords: barium nickel ferrite; ftir spectra; Debye temperature; force constants.

Classification: DDC Code: 543.56 LCC Code: QD96

Language: English

London Journals Press

LJP Copyright ID: 392924
Print ISSN: 2631-8474
Online ISSN: 2631-8482

London Journal of Engineering Research

Volume 22 | Issue 8 | Compilation 1.0

FTIR Spectra Analysis of Zinc Substituted Barium Nickel Ferrite

Sadiq. H. Khoreem [α], A. H. AL-Hammadi[σ] & W. F.Al-Eryani[ρ]

ABSTRACT

Nano - crystalline BaNix-2ZnxFe16O27 (where x = 0.0, 0.4, 0.8, 1.2, 1.6, and 2.0) w-type hexa-ferrite samples were generated using the typical standard ceramic methodology. Fourier transform infrared spectroscopy (FTIR) is a method which is used to identify the characteristic functional groups from the spectral bands that allow us to know the conjugation between the nanoparticles and the adsorbed biomolecules. It is used to detect different functional groups in Barium ferrites. The FTIR spectrum is recorded between 400 and 4000 cm^{-1}. The result shows the two main bands of absorption. The high-frequency band in the range 550-600 cm^{-1} and a low-frequency band at around 400 cm^{-1} were assigned to tetrahedral v_1 and octahedral v_2 sites, respectively, which illustrated the formation of the ferrite phase.

These two prominent bands are attributed to the intrinsic vibrations of tetrahedral and octahedral metal- oxygen bands in the crystal lattices of the BaNix-2ZnxFe16O27 hexagonal ferrite, respectively high frequency and low-frequency band . These two prominent peaks indicate the formation of hexa-ferrite. The stretching vibrations of metal-oxygen bonds is the reason for these peaks. The force constants (F_{Cons}) were calculated for tetrahedral F_{tet} sites and octahedral F_{oct} sites and were found to decrease with increasing Zn ions. The observed decrease in θ_D with zinc concentration suggests enhancement of the lattice vibrations due to Zn substitution. It can be seen that θ_D decreases with increasing Zn concentration.

Keywords: FTIR Spectra; Barium-Nickel ferrite; Debye temperature; Force constants.

Author α: Department of Optical and Vision Sciences, Faculty of Medicine, Al-Razi University, Sanaa, Yemen.

σ: Physics Department, Faculty of Science, Sana'a University, Sana'a, Yeme.

ρ: Physics Department, Faculty of Science, Saada University, Saada, Yemen.

I. INTRODUCTION

The improvement of ferrite nanoparticles' electrical and magnetic properties, as well as their good physical features, has given them confidence and the ability to have a lot of interest in their study. The w- type Hexa-ferrites have been used in a wide range of scientific, technological, and industrial applications, including those for humidity sensors, recording disks, microwave devices, catalysts, information storage, magnetic resonance imaging, ceramic coatings for solar cells, optoelectronic devices, and electronic devices. [1,–2]. Due to their sensible transmission in the optical portion of the spectrum as compared to other categories of materials, the optical characteristics of dielectric materials in general attracted attention. The optical constants, such as the absorption coefficient, transmission, reflection, and index of refraction, are crucial characteristics to explain the optical properties of ferrite materials[1,2].

The optical properties of the dielectric materials generally became of interest because of their Sensible transmission within the optical part of the spectrum as compared with different categories of materials. So that to study the optical properties of the ferrite materials, the optical constant such as absorption coefficient, transmission, reflection, and index of refraction are vital parameters to explain the optical properties of the ferrite materials [3]. The reportable by NARANG et al. about the Ni-Zn ferrites was different by the substitution of Zn^{2+}, ions, which prefer tetrahedral sites, with divalent

metal ions that either adopt octahedral positions or inhibit grain growth, and the magnetic properties were tailored with careful addition [4].

SHAUKAT, S. F., et al. reported the Cr-substituted W-type hexaferrite for the chemical composition (BaNi2CrxFe16-xO27.IR spectrum for sample revealed two well-defined absorption peaks which correspond to tetrahedral A- and octahedral B-sites present in W-type hexagonal lattice [5]. Muajsam, et al. synthesis the Ba-doped Co–Zn ferrite nanoparticles using the sol-gel auto combustion technique. The single-phase formation of the samples with F*d*3m space group was confirmed by X-ray diffraction (XRD) and fourier transformation infrared (FTIR) spectra display presence of two strong peaks around 430 cm^{-1} and 580 cm^{-1} that proved the formation of ferrite structure [6]. The general behavior for the nickel ferrites prefers to occupy the octahedral sites while the zinc prefers to occupy the tetrahedral site. The interactions between the tetrahedral ions and octahedral sites will alter the electrical and magnetic properties of ferrites. The octahedral sites are occupied by Ni^{2+} and $Fe^{3+,}$ whereas the tetrahedral sites are occupied through Zn^{2+} and Fe^{3+}. The properties of the ferrite are also strongly dependent on the synthesis method, sintering temperature, chemical composition, and so on. [7–9]. The infrared spectroscopic technique is based upon the fact that a chemical substance shows marked selective absorption in the infrared region.

Various bands present in the IR spectrum correspond to the characteristic functional groups and bonds present in the chemical substance. The infrared spectra are useful for determining the local symmetry and noncrystalline solids and studying the ordering phenomena in ferrite. In the present study, we investigated and discussed the fourier Fourier transformation infrared (FT-IR) spectra of the BaNix-2ZnxFe16O27 Hexagonal ferrites, where x = 0.0 ,0.4 0.8, 1.2, 1.6 and 2) 1.0 in the step of 0.20, which have been synthesis by the ceramic method.

II. MATERIALS AND METHODS

The samples used in this work had been prepared by the well-known ceramic method. with a high purity of BaCO3, ZnO, NiO, and Fe2O3 had been mixed according to their molecular weight ratio to obtain different compositions according to the following relation.

BaCo3+(2-x)(NiO)+x(ZnO)+8Fe2O3-»BaNi(2-x) .ZnxFe16O27+CO2↑

where x = 0.0, 0.4, 0.8, 1.2, 1.6, and 2. The weights of the mixed oxides in grams for each composition of the prepared system BaNi2-xZnxFe16O27. The oxides have been mixed and ground to a fine powder using a gate mortar made of carborundum for one hour for each sample, and then each sample was grounded again for five hours using a mechanical grinding machine. The mixture powder was pre-sintered in the air at 950 °C± 10°C for six hours after which it slowly cooled to room temperature. The aggregate was grounded again for five hours for each sample with the usage of the mechanical grinding gadget to get a totally nice powder. After that it was sintered at 1250°C± 10°C for 4 hours and slowly cooled to room temperature. The samples were made according to the technique of Stimson and Schiedt; 2.5 mg of the ferrite was mixed with 0.8 g of powdered KBr, and placed in a cylindrical die of 20 mm diameter. Then pressed for about 10 min at 18 tons/cm^2. C1ear disks of approximately 1 mm thickness were obtained with the usable transmission. FT-IR spectra of finely fine powder of all the compositions were recorded in the range of 4000 cm^{-1} to 400 cm^{-1}, measurements were made at room temperature.

III. RESULTS AND DISCUSSION

The formation of the surface functional group was confirmed by IR spectroscopy. To detect the metal-oxygen bond of the formed hexagonal BaNix-2ZnxFe16O27 phase materials, A few milligrams of BaNix-2ZnxFe16O27 powder mixed with anhydrous KBr powder and made in the form of a pellet for measurement. The FT-IR spectra were analyzed in the wavenumber range between 4000 and 400 cm^{-1} for the samples

shown in Figure 1. Generally, Figure 1. and Table.1, displays that each one the samples have M – O (metallic-oxygen) bond and the C = O bond. This proves a bond between the Fe, Ba, Ni, and Zn metals with oxygen in the specimen. The sample exhibits absorption bands from the ferrite compounds. Generally, two significant peaks can be observed at (430 - 439.69 &580 - 595 cm^{-1}) are observed. The peaks appearing between 400 and 600 cm^{-1} are the result of the vibration of metal-oxygen bond, which gives the idea of the formation of the ferrite phase[10].

These two prominent bands are attributed to the intrinsic vibrations of tetrahedral and octahedral metal- oxygen band in the crystal lattices of the Ba Nix-2 Zn Fe 16 27 hexagonal ferrite, respectively high frequency and low-frequency band [11-13]. These two prominent peaks indicate the formation of hexaferrite. The stretching vibrations of metal-oxygen bonds is the reason for these peaks.

The absorption peak at 1430 cm^{-1} is due to C–O asymmetric stretching vibration in the BaCO3. The absorption bands peaks around 1624cm^{-1} and 3449 cm^{-1} are due to stretching vibrations of water mode O-H. The H–O–H and O–H stretching vibration at wavenumbers around 3342 cm^{-1} and 1664 cm^{-1} due to the water and polyol in the precursor [14,15]. Bands located at 3435 cm^{-1} and 1590 cm^{-1} are due to the presence of O-H stretching vibration of (O– H) group of residual water and anti-symmetrical stretching vibration of CO2, respectively [16]. Also are assigned to stretching and bending vibration of H2O absorbed from the atmosphere when the samples were kept and ground in the air due to the high surface area of these materials [17]. The peak at 2348 cm^{-1} occurs as a result of the presence of CO2 in the prepared sample [18].

The absorption band at 2900 cm^{-1} is assigned to the C–H stretching vibration [19]. The band positions v1-v2 increase slightly as x increases; this is due to the fact that Zn^{2+} is lighter atomic weight compared to host Ni^{2+}, and that the wavenumber is inversely proportional to the atomic weight [20].

3.1 Force constants

The variation in wavenumbers (ν_1& ν_2) with zinc concentration(x) for all samples is shown in Figure 2.a. From the figure.2.a, it has been observed that the ν_2 shift towards lower frequencies however, ν_1 shift towards higher frequencies with zinc concentration (x) is expected because of a large ionic radius of Zn^{2+} ion samples [21]. The values of the force constants (Ftet and Foct) for the band Fe^{3+} - O^{2-} at tetrahedral and octahedral sites are calculated using the relation [22,23].

$$Ftet = 4\,\pi^2 c^2 \nu_1^2\,\mu \quad (1)$$

$$Foct = 4\pi^2 c^2 \nu_2^2 \mu \quad (2)$$

where Ftet is the tetrahedral force constant and Foct is the octahedral force constant, and c=2.99x10^{10} cm/s, is the speed of light, whereas ν_1 and ν_2 is the band wavenumber in cm^{-1} and μ is the reduced mass for Fe^{3+} ions and O^{2-} ions (2.061x10^{-23} g).

The values of force constant for tetrahedral (Ftet) and octahedral (Foct) sites are listed in Table 1. The variety in force constant with zinc concentration(x) for all samples at tetrahedral and octahedral sites was displayed in Figure 2.b.

From the figure.2.b, it is observed that Ftet declines with an increase in zinc ion concentration. This conduct can be attributed to the variety in cation oxygen bond length [24].

Since the bond length (A-O) increased with an expansion in zinc concentration, the energy required to break longer bonds is less, supporting a decrease in the force constant of tetrahedral sites.

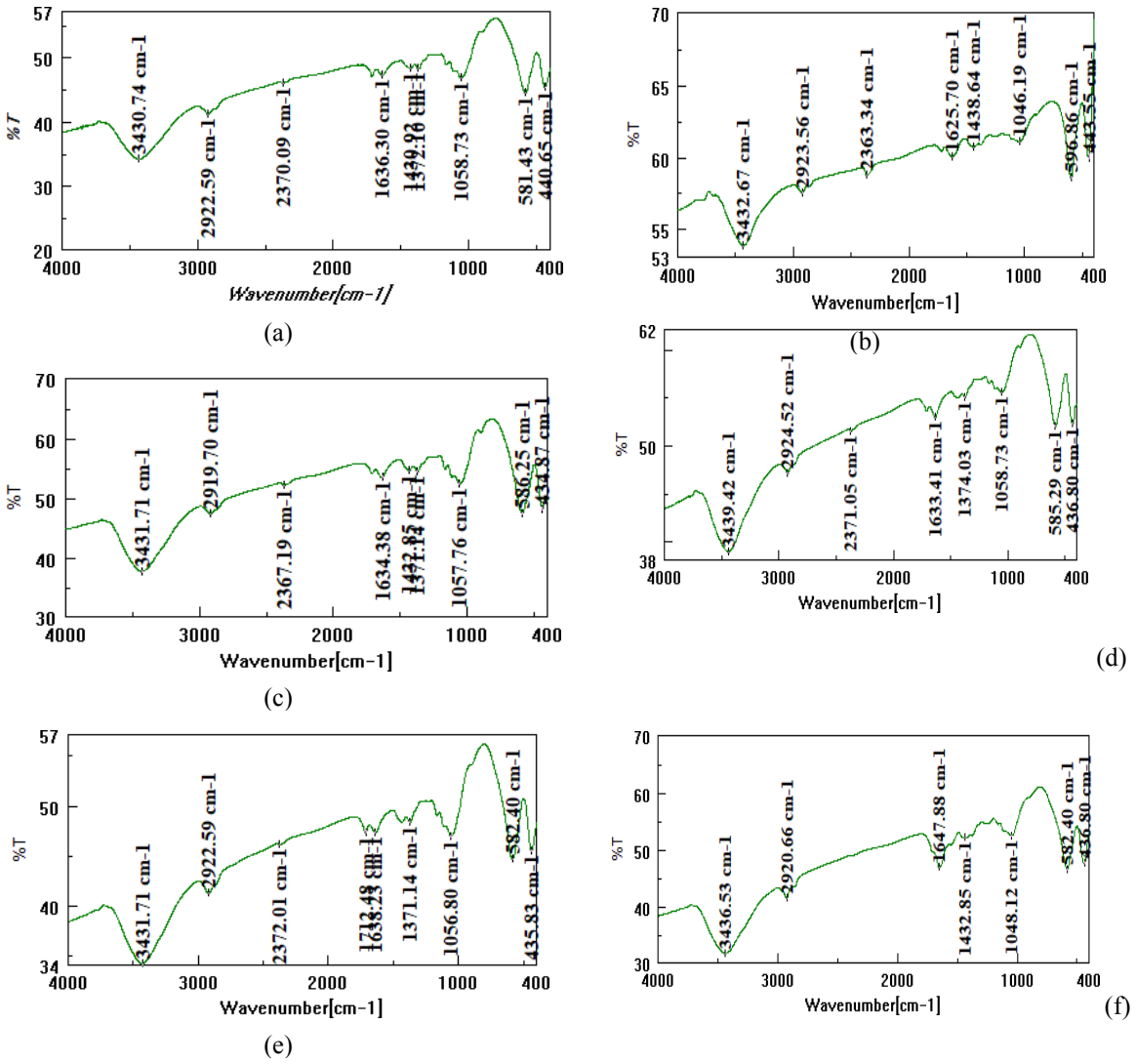

Figure 1: (a,b,c,d,andf) IR pattern BaNix-2ZnxFe16O27 (x = 0, 0.4, 0.8, 1.2, 1.6 & 2) ferrites. (a) x=0.0; (b) x=0.4;. (c) x=0 .8; (d) x=1.2; (e) x=1.6; (f) x=2.0

The change in the band position is due to the change in the Fe^{3+}-O^{2-} internuclear distances for the tetrahedral and octahedral sites, respectively [25,26]. Normally, it is expected that a rise in band length ought to result in a decrease in force constant. If the radius of the impurity ion is larger than the displaced ion, then the bond length increases, lowering the force constant for either site or a reduction in the repulsive forces between the ions leading to lower electrostatic energy implying a lower wavenumber. The reverse will hold if a smaller impurity ion replaces a metal ion of the regular lattice. A decrease in wavenumber and force constant is expected with zinc substitution because of its larger ionic radius(0.74Å) than the displaced Ni^{2+} ion (0.69 Å) [14]. The positions of absorption bands in terms of wavenumber vtet and voct for all samples are summarized in table_ 1. From Table 1, it is clear that the position of the vtet and voct band is shifted with the incorporation of Zn ions in the Ni matrix. The same behavior was reported in previous work of different ferrite systems [27,28]. FT-IR results clearly indicate that Ni ions are stabilized in the Oh crystal field, whereas Zn ions prefer Td sites because of their ability to form covalent bonds [29-32]. The small shift in band positions for Ba-Zn-Ni ferrites is observed as a function of Zn content (x) (Table 1), and it may be caused by differences in the ionic distances Fe B-O and Fe A-O, which are equal to 0.199 nm and 0.189 nm respectively [33]. This reason can also cause the stronger covalent bonding of Fe^{3+} ions at the tetrahedral sites than at the octahedral sites.

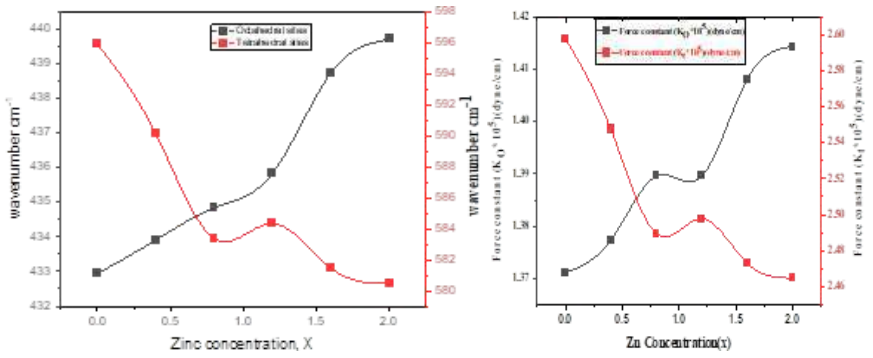

Figure 2: (a)Variation of wave numbers at A and B sites with zinc concentration. (b) force constants with Zinc concentration (x) at tetrahedral and octahedral site.

Debye temperature is an essential parameter to study lattice vibrations [34]. The Debye temperature (θD) for BaNix-2ZnxFe16O27 (x = 0, 0.4, 0.8, 1.2, 1.6, 2) ferrites was obtained by using the next relation [35,36]

$$\theta_D = \frac{hc\nu_{av}}{K_B}$$

where h is Plank constant (h = 6.626 ×10^{-34} J.s), KB is Boltzmann constant (KB =1.3806×10^{-23} J K^{-1}), c is velocity of light (c =2.99 ×10^{10} cm s^{-1}) and vav is average wave-number of bands (cm^{-1}).

The calculated values of the debye temperature (θD)for the samples are depicted in figure.3. It can be noticed that with increasing zinc content θD decreases from 738.19 K (for x = 0.0; to 731.96 K (for x = 1.2), and after that remains constant. These values have a great importance to determine the conduction mechanism of these ferrites. It can be linked to a decrease in wavenumber of the peak usually attributed to Me-O bond vibration in the tetrahedral site. The observed decrease in θD (Table 1) with zinc concentration suggests enhancement of the lattice vibrations due to Zn-substitution. It can be seen that θD decreases with increasing Zn concentration.

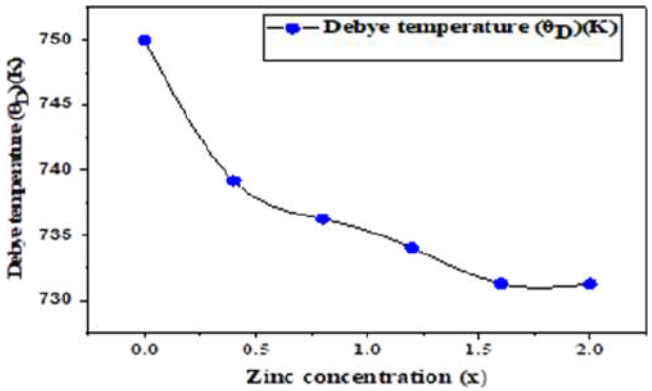

Figure 3: Variation Debye temperature (θ_D)(K)with increasing Zinc concentration (x)

These behaviors can be discussed based on a specific heat theory. According to this theory, electrons absorb part of the heat and θD may decrease with increasing zinc ions concentration; this suggests that the conduction for these samples is due to electrons (i.e., n- type) [37].

Table 1: Calculated force constants of tetrahedral and octahedral sites; Debye temperature

Composition	Absorption band (Wave number)	Force constants	Absorption band (Wave number)	Force constants	Debye temperature (θ_D)
x	v_2 (cm^{-1})	F_{octa} dyn/cm (x 10^5)	v_1 (cm^{-1})	F_{tet} dyn/cm (x 10^5)	θ_D (K)
X=0	432.94	1.36139	595.86	2.57910	738.1946
X=0.4	433.905	1.36747	590.111	2.52927	734.7363
X=0.8	434.834	1.37333	583.31	2.47174	730.5597
X=1.2	435.834	1.37965	584.35	2.47992	731.9688
X=1.6	438.726	1.39802	581.43	2.45543	731.9688
X=2	439.69	1.40417	580.49	2.44729	731.96888

IV. CONCLUSIONS

FT-IR spectra of the samples have been analyzed in the frequency range (400-4000) cm^{-1}. The two main bands of absorption corresponding to tetrahedral *v1* and octahedral *v2* were observed, which illustrated the formation of the ferrite phase. The high-frequency band in the range, 550-600 cm^{-1} and a low-frequency band at around 400 cm^{-1} were assigned to tetrahedral *v1* and octahedral *v2* sites, respectively. The force constants were calculated for tetrahedral Ftet sites, and octahedral Foct sites and frequencies show that Kt decreases with tetrahedral bond length and KO increases with octahedral bond length.with increasing Zn ions. Debye temperature (θD) has also been estimated as a function of composition at room temperature using FTIR spectra. The behavior of Debye temperature θ_D showed that electrons should make a significant contribution to the specific heat.

Conflicts of Interest

The authors declare no conflict of interest."

REFERENCES

1. Dhiman, P.; Jasrotia, R.; Goyal, D.; Mola, G.T. Hexagonal Ferrites, Synthesis, Properties and Their Applications. Ferrite: Nanostructures with Tunable Properties and Diverse Applications 2021, 112.
2. Bharati, V.A.; Somvanshi, S.B.; Humble, A.V.; Murumkar, V.D.; Sondur, V.V.; Jadhav, K.M. Influence of trivalent Al–Cr co-substitution on the structural, morphological and Mössbauer properties of nickel ferrite nanoparticles. Journal of Alloys and Compounds 2020, 821, https:// doi.org/10.1016/j.jallcom.2019.153501.
3. Kulkarni, A.B.; Mathad, S.N. Effect of cadmium doping on structural and magnetic studies of Co-Ni ferrites. Science of Sintering 2021, 53, 407-418.
4. Narang, S.B.; Pubby, K. Nickel Spinel Ferrites: A review. Journal of Magnetism and Magnetic Materials 2021, 519, https://doi.org/10.1016/j.jmmm.2020.167163.
5. Rehman, A.u.; Shaukat, S.F.; Haidarah, A.S.; Akhtar, M.N.; Ahmad, M. Synthesis and investigations of structural, magnetic and dielectric properties of Cr-substituted W-type Hexaferrites for high frequency applications. Journal of Electroceramics 2021, 46, 93- 106, https://doi.org/10.1007/s10832-021-00246-7.
6. Batoo, K.M.; Hadi, M.; Verma, R.; Chauhan, A.; Kumar, R.; Singh, M.; Aldossary, O.M. Improved microwave absorption and EMI shielding properties of Ba-doped Co–Zn ferrite. Ceramics International 2022, 48, 3328-3343, https://doi.org/10.1016/j.Ceramint.2021.10.108.
7. Costa, A.C.F.M.; Silva, V.J.; Cornejo, D.R.; Morelli, M.R.; Kiminami, R.H.G.A.; Gama, L. Magnetic and structural properties of NiFe2O4 ferrite nanopowder doped with Zn2+. Journal of Magnetism and Magnetic Materials 2008, 320, e370-e372, https://doi.org/10.1016/j.jmmm.2008.02.159.
8. AL-Hammadi , A.H.; Khoreem , Sadiq H. Investigations on Optical and Electrical Conductivity of Ba/Ni/Zn/Fe16O27 Ferrite Nanoparticles. Biointerface Res Appl Chem 2022, 13, 168, doi:10.33263/BRIAC132.168.

9. Sattibabu, B.; Rao, T.D.; Das, T.; Chatterjee, M.; Bhatnagar, A.K.; Rayaprol, S.; Das, D. Synthesis and magnetic properties of nanostructured Ni1-xZnxFe2O4 (x = 0.4, 0.5 and 0.6). AIP Conference Proceedings 2020, 2269, https://doi.org/10.1063/5.0019566.
10. Tchouang, T.C.T.; Sharma, J.; Mohammed, J.; Kumar, S.; Srivastava, A.K. Effect of temperature on the magnetic properties of nano-sized M-type barium hexagonal ferrites. AIP Conference Proceedings 2017, 1860, https://doi.org/10.1063/1.4990307.
11. Zhang, C.; Shi, J.; Yang, X.; De, L.; Wang, X. Effects of calcination temperature and solution pH value on the structural and magnetic properties of Ba2Co2Fe12O22 ferrite via EDTA-complexing process. Materials Chemistry and Physics 2010, 123, 551-556, https://doi.org/10.1016/ j.matchem phys.2010.05.013.
12. Ramzan, M.; Arshad, M.I.; Mahmood, K.; Amin, N.; Khan, M.I.; Iqbal, F.; Ajaz-un-Nabi, M. Investigation of Structural and Optical Properties of Pr3+-Substituted M-Type Ba–Ni Nano-Ferrites. Journal of Superconductivity and Novel Magnetism 2021, 34, 1759-1764, https://doi.org/10.1007/s10948-020-05751-4.
13. Mosleh, Z.; Kameli, P.; Poorbaferani, A.; Ranjbar, M.; Salamati, H. Structural, magnetic and microwave absorption properties of Ce-doped barium hexaferrite. Journal of Magnetism and Magnetic Materials 2016, 397, 101-107, https://doi.org/10.1016/j.jmmm.2015.08.078.
14. Fatima, N.; Khan, H.M.; Laref, A.; Alhashim, H.H.; Zahid, M.; Nadeem, M.; Akhtar, T.; Anjum, R. Synthesis And Characterization Of Cobalt Substituted W Type Hexagonal Ferrites. Digest Journal of Nanomaterials & Biostructures (DJNB) 2021, 16.
15. Huang, X.; Zhang, J.; Wang, L.; Zhang, Q. Simple and reproducible preparation of barium hexagonal ferrite by adsorbent combustion method. Journal of Alloys and Compounds 2012, 540, 137-140, https://doi.org/10.1016/j.jallcom.2012.05.015.
16. da Costa Lima, R.; Pinho, M.S.; Ogasawara, T. Thermal characterization of the intermediary products of the synthesis of Zn-substituted barium hexaferrite. Journal of Thermal Analysis and Calorimetry 2009, 97, 131, https://doi.org/10.1007/s10973-009- 0256-4.
17. Simonescu, C.M.; Tătăruş, A.; Culiţă, D.C.; Stănică, N.; Butoi, B.; Kuncser, A. Facile Synthesis of Cobalt Ferrite (CoFe2O4) Nanoparticles in the Presence of Sodium Bis (2- ethyl-hexyl) Sulfosuccinate and Their Application in Dyes Removal from Single and Binary Aqueous Solutions. Nanomaterials 2021,11, https://doi.org/10.3390/nano11113128.
18. Davarpanah, E.; Armandi, M.; Hernández, S.; Fino, D.; Arletti, R.; Bensaid, S.; Piumetti, M. CO2 capture on natural zeolite clinoptilolite: Effect of temperature and role of the adsorption sites. Journal of Environmental Management 2020, 275, https://doi.org/10.1016/j.jenvman.2020.111229.
19. Barbe, A.; Mikhailenko, S.; Starikova, E.; Teterev, V. Infrared spectra of 16O3 in the 900 - 5600 cm−1 range revisited: Empirical corrections to the S&MPO and HITRAN 2020 line lists. Journal of Quantitative Spectroscopy and Radiative Transfer 2021, 276, https://doi.org/10.1016/j.jqsrt.2021.107936.
20. Chavan, V.C.; Shirsath, S.E.; Mane, M.L.; Kadam, R.H.; More, S.S. Transformation of hexagonal to mixed spinel crystal structure and magnetic properties of Co2+ substituted BaFe12O19. Journal of Magnetism and Magnetic Materials 2016, 398, 32-37, https://doi.org/10.1016/j.jmmm.2015.09.002.
21. Balavijayalakshmi, J.; Suriyanarayanan, N.; Jayaprakash, R. Effects of sintering on structural and magnetic properties of Cu substituted cobalt–nickel mixed ferrite nanoparticles. Journal of Magnetism and Magnetic Materials 2014, 362, 135-140, https://doi.org/10.1016/j.jmmm.2014.03.005.
22. Raje Shaikh, B.B.; Chishty, S.Q. Auto-ignition synthesis of rare-earth metal-doped Ni– Zn spinel ferrites for electronic applications. Journal of Materials Science: Materials in

Electronics 2021, 32, 23999-24010, https://doi.org/10.1007/s10854-021-06863-w.
23. Chacko, B.; Roy, A.; Melbin Richard, A.; Swathy, J.; Avanish, B.T.; Madhuri, W. Bismuth modified zinc ferrites for low-temperature ceramic co-firing technology. Materials Chemistry and Physics 2022, 276, https://doi.org/10.1016/j.matchemphys.2021.125401.
24. Ladgaonkar, B.P.; Kolekar, C.B.; Vaingankar, A.S. Infrared absorption spectroscopic study of Nd3+ substituted Zn-Mg ferrites. Bulletin of Materials Science 2002, 25, 351- 354, https://doi.org/10.1007/BF02704131.
25. Shannon, R.D. Revised effective ionic radii and systematic studies of interatomic distances in halides and chalcogenides. Acta Crystallographica Section A 1976, 32, 751-767, https://doi.org/10.1107/S0567739476001551.
26. Warhate, V.V.; Badwaik, D.S.; Chopne, S.R. Thermal and infrared spectral analysis of TiCo doped NiZn Y-type strontium hexaferrite synthesized by sol gel auto-combustion. Materials Today: Proceedings 2020, 29, 1055-1058, https://doi.org/10.1016/j.matpr.2020.04.712.
27. Abou-Elsaad, N.I.; Nawara, A.S.; Mazen, S.A. Synthesis, structural characterization, and magnetic properties of Ni–Zn nanoferrites substituted with different metal ions (Mn2+, Co2+, and Cu2+). Journal of Physics and Chemistry of Solids 2020, 146, https://doi.org/10.1016/j.jpcs.2020.109620.
28. Abul-Magd, A.A.; Morshidi, H.Y.; Abdel-Ghany, A.M. The role of NiO on the structural and optical properties of sodium zinc borate glasses. Optical Materials 2020, 109, https://doi.org/10.1016/j.optmat.2020.110301.
29. Dawoud, H.A.; Abu Ouda, L.S.; Shaat, S.K. FT-IR studies of nickel substituted polycrystalline zinc spinel ferrites for structural and vibrational investigations. Chemical Science Transactions 2017, 6.
30. Aly, K.I.; Sayed, M.M.; Mohamed, M.G.; Kuo, S.W.; Younis, O. A facile synthetic route and dual function of network luminescent porous polyester and copolyester containing porphyrin moiety for metal ions sensor and dyes adsorption. Microporous and Mesoporous Materials 2020, 298, https://doi.org/10.1016/j.micromeso.2020.110063.
31. Venkataraju, C.; Paulsingh, R. FTIR and EPR Studies of Nickel Substituted Nanostructured Mn Zn Ferrite. Journal of Nanoscience 2014, 2014, 1-5, https://doi.org/10.1155/2014/815385.
32. Kargar, H.; Behjatmanesh-Ardakani, R.; Torabi, V.; Sarvian, A.; Kazemi, Z.; Chavoshpour-Natanzi, Z.; Mirkhani, V.; Sahraei, A.; Nawaz Tahir, M.; Ashfaq, M. Novel copper(II) and zinc(II) complexes of halogenated bidentate N,O-donor Schiff base ligands: Synthesis, characterization, crystal structures, DNA binding, molecular docking, DFT and TD-DFT computational studies. Inorganica Chimica Acta 2021, 514, https://doi.org/10.1016/j.ica.2020.120004.
33. Ardit, M.; Zanelli, C.; Conte, S.; Molinari, C.; Cruciani, G.; Dondi, M. Ceramization of hazardous elements: Benefits and pitfalls of inertisation through silicate ceramics. Journal of Hazardous Materials 2022, 423, https://doi.org/10.1016/j.jhazmat.2021.126851.
34. Modi, K.B.; Raval, P.Y.; Shah, S.J.; Kathad, C.R.; Dulera, S.V.; Popat, M.V.; Zankat, K.B.; Saija, K.G.; Pathak, T.K.; Vasoya, N.H.; Lakhani, V.K.; Chandra, U.; Jha, P.K. Raman and Mossbauer Spectroscopy and X-ray Diffractometry Studies on Quenched Copper–Ferri–Aluminates. *Inorganic Chemistry* 2015, 54, 1543-1555, https://doi.org/10.1021/ic502497a.
35. Tatarchuk, T.; Bououdina, M.; Macyk, W.; Shyichuk, O.; Paliychuk, N.; Yaremiy, I.; Al-Najar, B.; Pacia, M. Structural, Optical, and Magnetic Properties of Zn-Doped CoFe2O4 *Nanoparticles*. *Nanoscale Research Letters* 2017, 12, 141–151, https://doi.org/10.1186/s11671-017-1899-x.
36. Tatarchuk, T.R.; Paliychuk, N.D.; Bououdina, M.; Al-Najar, B.; Pacia, M.; Macyk, W.; Shyichuk, A. Effect of cobalt substitution on structural, elastic, magnetic and optical properties of zinc ferrite nanoparticles. *Journal of Alloys and Compounds* 2018, 731,

1256-1266, https://doi.org/10.1016/j.Jallcom.2017.10.103.
37. Gamal, W.M.; El-Bassiouny, A.A.H.; Abdelsalam, H.K.; Wahab, S.M.A.E. Role of elastic and optical properties on silver nanoferrite and nanochromis for optical switch device applications. Journal of Materials Science: *Materials in Electronics* 2021, 32, 21590-21602, https://doi.org/10.1007/s10854-021-06667-y.